Quantifying Energy-Efficient Evolution in Cursorial Avian Archosaurs Through Comparative Torque-Based Hindlimb Modeling

Sarva Vohra

Affiliation: Independent Researcher, Waxhaw, North Carolina, United States of America

Corresponding Author: Sarva Vohra (sarva.vohra.research@gmail.com),

ORCID: 0009-0000-1688-3459

This paper is currently a non-peer-reviewed preprint submitted to EcoEvoArXiv.

Quantifying Energy-Efficient Evolution in Cursorial Avian Archosaurs Through Comparative Torque-Based Hindlimb Modeling

Sarva Vohra

Affiliation: Independent Researcher, Waxhaw, North Carolina, United States of America

Corresponding Author: Sarva Vohra (sarva.vohra.research@gmail.com),

ORCID: 0009-0000-1688-3459

Abstract:

Understanding the way evolution drives adaptations that "optimize" energy-efficiency in cursorial species provides instrumental insights into both biomechanical and bio-inspired engineering fields. This study quantitatively models the cursorial evolution of energy-efficient locomotion in bird-line archosaurs by comparing the hindlimb mechanics of *Deinonychus antirrhopus* (extinct theropod) and *Struthio camelus* (modern ostrich). A Python-based two-dimensional framework was constructed to evaluate static torque and dynamic stride simulations across joint angles and skeletal lengths. Joint torque and quadriceps force (F_{quad}) were computed using vector-based external moment equations, nonlinear passive stiffness (k_1 and k_3), and normalized body-weight scaling. Sensitivity analyses were conducted on center-of-mass position, patellar tendon moment arm, and knee rest angle to assess model robustness. Results demonstrated that *S. camelus* exhibited a broader region of minimized F_{quad} and smoother torque fluctuations (which are indicative of a more "optimized" energy-efficient, extended posture), whereas *D. antirrhopus* required a greater muscular effort due to its intrinsic crouched posture. Across both static and dynamic conditions, a greater vertical limb orientation consistently reduced the magnitude of F_{quad}, confirming that distal limb elongation and posture evolution—key characteristics of cursorial evolution—enhanced mechanical efficiency. This study provides quantitative evidence that avian cursorial evolution can be mapped as an optimization of locomotor efficiency, offering a quantitative framework for translating evolutionary principles into energy-efficient robotic and prosthetic innovation.

Keywords: biomechanics; cursorial evolution; evolutionary modeling; optimization; paleobiology; archosaurs; quadriceps force

Introduction:

Evolution is theorized as a powerful force in biological optimization; through natural selection, organisms appear optimized for specific functions that maximize fitness or minimize energetic cost. In bio-locomotive applications, organisms are assumed to move towards energy-efficient configurations, allowing them to divert excess energy and resources to key functions of survival (e.g., the reproductive systems) (Parker & Maynard Smith, 1990). This assumption is derived from evolutionary theory that posits natural selection will drive systems to a relative optimization for their environments.

This paper focuses on cursorial evolution—terrestrial locomotion adaptations and trends—in bird-line archosaurs, the group of animals inclusive of dinosaurs and modern birds. Cursorial adaptations in this lineage are characterized by limb elongations (specifically the tibia and metatarsus) to increase stride lengths, a shifted center of mass forward of the hip for stability, and adjusted joint alignment to a more vertical stance, minimizing torque and energy loss (Kubo, 2025; Hutchinson, 2006). These characterizations are presumed exemplifiers of a biological optimization process; bird-line archosaurs have evolved towards morphologies that minimize mechanical work (Allen et al., 2021).

Evolution's high regard as an optimization tool has allowed for interdisciplinary sciences to draw inspiration from organisms' locomotive systems. The famous Massachusetts Institute of Technology (MIT) Cheetah robot demonstrates robotic advancements derived from biological principles (Seok et al., 2015). Evolutionary processes inspire optimized mechanics in engineering fields, meaning evolutionary biology studies can hold a large weight beyond just biology (Castle et al., 2024).

While evolution has been qualitatively substantiated as an optimizational process, the absence of quantitative and dynamic models that link cursorial evolution to energetic optimization detracts from the mathematical and engineering applications of evolutionary biology (Bishop, 2021; Kocher, 2023). Earlier works—like Allen's 2013 anatomical reconstructions—describe limb posture evolution of extinct archosaurs, but do not numerically evaluate torque nor force efficiencies of postures. This lack of mechanical physics data limits the usability of taxa-based robotic models, as engineering fields are physics-heavy and dependent on the forces applied to these models.

To enhance and bolster robotic and engineering applications of evolutionary biology, this study bridges an existing gap through a numerical comparative analysis of quantitative torque optimization and stride cycles of two key archosaur species: *Deinonychus antirrhopus* and *Struthio camelus* (an extinct raptor species and the modern ostrich). As *D. antirrhopus* was a non-avian theropod, it holds strong links to modern birds, allowing for a stronger comparative analysis. *S. camelus* was chosen for its representation as a large flightless modern archosaur and its prevalence in biomechanical and locomotive research. This

pairing enabled a quantitative tracking of locomotive efficiency between different stages of the archosaur lineage.

Completing a comparative analysis of two related taxa required comparisons between two key measures: joint torque and quadriceps force demand. Joint torque represents the rotational force needed to support a normalized body weight at each joint, capturing the mechanical efficiency of a species. Quadriceps force (F_{quad}) quantified biological effort—the muscular output required for stability and locomotion. To derive these values, varying knee and ankle angles were iterated through to conceptualize when joint torque and F_{quad} would be at their minimum values, which would indicate a level of optimization. It was hypothesized that *S. camelus* would exhibit lower joint torques and reduced quadriceps force demands across a range of stance and stride postures when normalized and compared to *D. antirrhopus*, reflecting an evolutionary shift towards mechanically optimized, energy-efficient locomotion in cursorial birds.

By bridging paleobiology, comparative anatomy, and engineering design principles, hypotheses and justifications of the validity of cursorial evolution's optimization capabilities were made and supported. Demonstrating how limb proportion and joint angle shifts influenced the energetic efficiency of a taxon links paleontological data to modern engineering design; the quantitative measurements presented in this paper have the potential to be implemented into robotics development labs to create optimized, energy-efficient devices.

Note: While this study models evolutionary change as an optimization process to analyze biomechanical efficiency, evolution itself does not act with intent or foresight. The "optimization" described here is a heuristic representation of how natural selection can favor energetically efficient traits over millions of years, rather than a literal goal-driven mechanism (Parker & Maynard Smith, 1990; Castle et al., 2024). Evolutionary dynamics are complex and do not have an aim, nor do they select for the most optimal organism.

Methodologies:

This study employed a three-step comparative computational biomechanics framework combining static torque analysis, dynamic stride simulation, and sensitivity testing. All computations were implemented in Python 3.11 using NumPy 1.26 and Matplotlib 3.8. Forces were normalized to body weight (BW) and lengths to femur length (Lf) for interspecific comparability.

2.1 Static Torque Optimization—Determination of Optimal Hindlimb Posture via Static Torque Analysis

This section details the methodology used to calculate static torque across varying hindlimb joint angles in *Deinonychus antirrhopus* and *Struthio camelus*. Using rotational dynamics and matrix-based angle analysis, the aim was to identify knee and ankle configurations where quadriceps force and joint torque are minimized, providing a quantitative measure of mechanical efficiency during stance.

2.1.1 Model Reconstruction

The hindlimb reconstruction of *D. antirrhopus* was modeled as a four-segment kinematic chain consisting of the femur, tibia, metatarsus, and phalanges. As accurate skeletal measurements of extinct taxa are limited, non-primary bones were condensed into the primary four segments. Each of these segments was modeled as a rigid rod connected by hinge joints representing the hip, knee, ankle, and metatarsophalangeal (MTP) joints. Bone proportions were determined from Dr. Scott Hartman's skeletal references – a commonplace reference for extinct taxon reconstructions (Hartman, 2025). Fixated angles (hip and MTP) were predetermined using ostrich angles as a reference, and adjusting the angles for a more crouched theropod.

The extant species, *S. camelus*, was modeled in a manner similar to *D. antirrhopus*, but with skeletal and angular values derived from existing literature (Kassem, 2023; Rubenson, 2007). Segment lengths were expressed as ratios relative to the femur length to ensure cross-comparability across the different taxa. The respective centers of pressure (CoP) were positioned along the phalangeal rod as a fraction of phalanx length. The centers of mass (CoM) were fixed relative to the hip, which was positioned in a two-dimensional sagittal plane, with the hip joint at the origin, the x-axis representing horizontal displacement, and the y-axis representing vertical displacement. Values for each taxa's skeletal ratios, CoP, and CoM are found in Table 1.

2.1.2 Coordinate System and Kinematic Calculations

Segment endpoints (the positions of the knee, ankle, MTP, and CoP) were calculated using forward kinematics (Smith, 2007). The respective joint positions were computed as a cumulative sum of vector components that were derived from ratio segment lengths and input joint angles. For example, the position of the knee and the subsequent position of the ankle were calculated as follows:

$$P_{knee} = \left[L_{femur} cos(\theta_{Hip}),\ L_{femur} sin(\theta_{Hip})\right]$$

$$P_{ankle} = P_{knee} + \left[L_{tibia} cos(\theta_{Hip} - \theta_{knee}),\ L_{tibia} sin(\theta_{Hip} - \theta_{knee})\right]$$

The same calculation was performed in iterations for the position of MTP and CoP, in accordance with input values and ratios previously determined by other locomotive studies (Regnault et al., 2017; Smith, 2007). All trigonometric operations were handled in radians as Python algorithms operate on radian values. Code Segment 1.1 details the Python equivalent of the preceding rotational dynamics equations.

This iterative kinematic model provided the positional foundation for subsequent torque and muscle-force calculations (Section 2.1.3).

Code Segment 1.1

```
p_k = np.array([ self.femur_length*math.cos(th_h),
                 self.femur_length*math.sin(th_h) ], dtype=float)

p_a = p_k + (np.array([ self.tibia_length*math.cos(th_tib),
                        self.tibia_length*math.sin(th_tib) ], dtype=float))
```

2.1.3 Torque and Force Computation

The external moment about the knee was calculated using a two-dimensional vector cross-product, which defined the lever arm between the ground reaction force (GRF) vector and the knee joint. The GRF acts through the center of pressure, which was earlier defined as a fraction along the phalangeal segment, and the center of mass. The following equations were used:

$M_k^{req} = -(r_x F sin(\phi) - r_x F cos(\phi))$, where ϕ (the angle of the GRF vector) is derived from

$$arctan2(y_{CoM} - y_{CoP},\ x_{CoM} - x_{CoP}).$$

$$F_{quad} = \frac{\left|M_{tot} = M_k^{req} - M_{passive}\right|}{r_{PT}}, \text{ where } M_{passive} = k_1(\theta_k - \theta_0) + k_3(\theta_k - \theta_0)^3.$$

M_k^{req} is the torque the quadriceps must counteract to maintain posture. The vector from the knee to the CoP (the "lever arm") was defined as r. $M_{passive}$ represented the passive elastic support—modeled

through a standard nonlinear elastic torque formula—provided by tendons and ligaments, modeled in accordance with established biomechanical literature (Table 1) (Hosseinzadeh et al., 2020; Regnault et al., 2017). To make results comparable across species and sizes, torques and forces were normalized to body weight (BW) and femur length (L_{femur}).

To identify angle configurations where F_{quad} and joint torques were at a minimum, the preceding calculations were iterated over anatomically feasible ranges of angles. Knee angle values were run over 0° to 140°; ankle, 0° to 70°. Heatmaps were generated in Python to visualize the comparison between knee angles and ankle angles, and the respective force exerted by the quadriceps (F_{quad}). Code Segment 1.2 shows the Python equivalent of the iteration cycles. Heatmaps were produced using the `matplotlib` library import in Python.

Code Segment 1.2

```
angles_k = np.linspace(30, 140, 222) #knee angle θ_k (deg); sweeping 30-140, with 222 increments
ankles_a = np.linspace(0, 70, 142)   #ankle angle θ_a (deg); sweeping 0-70, with 142 increments
```

2.2 Dynamic Stride Simulation—Dynamic Simulation of One Stride Cycle

By extending the static torque model to dynamic conditions via a time-based stride simulation of *D. antirrhopus* and *S. camelus*, the quantification of the variation in joint torque and limb posture over a normalized gait was drawn to assess dynamic efficiency. In short, mapping the previous static findings onto dynamic conditions allowed for an analysis of knee torque and quadriceps force over one stride—the time it takes to complete one gait cycle.

2.2.1 Model Import and Kinetics & Temporal Inputs

The same model used for a static comparison—a four-segment kinematic chain linked by hinge joints—was used for a dynamic comparison. Skeletal ratios, angular defaults, and moment arm fractions remained consistent (Table 1).

To ensure cross-species comparability, stride durations were normalized, with $t \in [0, 1]$ across 200 frames. The stance percentage—the percent of time an animal's limb is in contact with the ground, and GRF is acting on the limb in one stride—was determined for *S. camelus* to be 40% using Rubenson's 2017 past locomotive study. For *D. antirrhopus*, the stance percentage was estimated to be 45%, a slight variation upward due to a similar, but more crouched posture compared to its modern counterpart.

2.2.2 Keyframes and Interpolation

To map how skeletal segments and joint angles act in a stride cycle, keyframes for the four main joint angles were set and bridged via cosine-eased interpolation. Keyframes are points of arbitrary time (ranging from 0-1) where the angles of the four joints of a hindlimb were fixed. Code Segment 2.1 shows the keyframe initializations for *S. camelus* and *D. antirrhopus*. Angles for *S. camelus* were derived using an image overlay and angle values from existing papers (Rubenson, 2007; Zhang et al., 2017). For *D. antirrhopus*, angle assumptions were derived from multiple existing literature sources, and logic-based assumptions (e.g., because *D. antirrhopus* had a more crouched posture, its angles would be less vertical than *S. camelus*'s). *D. antirrhopus* also had more keyframes to increase confidence and to ensure exact mapping—it had more locomotive fluctuations in a gait cycle than *S. camelus*.

Code Segment 2.1

```
#Keyframed joint trajectories (deg) D. antirrhopus
key_t = [0.00, 0.20, 0.40, 0.60, 0.80, 1.00]
theta_h   = smooth_keyframe_curve(t, key_t, [-30, -45, -75, -95, -60, -30])
theta_k   = smooth_keyframe_curve(t, key_t, [105,  95,  40,  50,  85, 105])
theta_a   = smooth_keyframe_curve(t, key_t, [ -80, -85, -10, -40, -95, -80])
theta_mtp = smooth_keyframe_curve(t, key_t, [ -55, -50, -90,   0,  30, -55])

---

#Keyframed joint trajectories (deg) S. camelus
key_t = [0.00, 0.50, 0.75, 1.00]
theta_h   = smooth_keyframe_curve(t, key_t, [-40, -50, -45, -40])
theta_k   = smooth_keyframe_curve(t, key_t, [ 47,  90,  90,  47])
theta_a   = smooth_keyframe_curve(t, key_t, [ -10, -45, -90, -10])
theta_mtp = smooth_keyframe_curve(t, key_t, [ -73,  15,  30, -73])
```

The `smooth_keyframe_curve` function allowed for a cosine-eased interpolation between the keyframes, keeping the stride's simulated movements smooth instead of linear. Through this, realistic extended-to-flexed limb transitions were generated that represented avian cursorial motion—a more complex measure of evolution than static motion.

2.2.3 GRF and Inverse Dynamics

GRF only acts on the foot during the stance phase; it represents the upward force exerted by the ground upward. As set earlier, GRF acts on the center of pressure (CoP). During the stance phase, GRF

does not act consistently, so its magnitude was modeled as a half-sine waveform, peaking at 1x body weight (BW), as we set in our initial parameters, which occurred midstance. This midstance position correlates with the same position where the optimal stationary angles take place. The use of a half-sine waveform allowed for a smooth fluctuation between the GRF's magnitude values (0-1), mirroring the way the GRF rises and falls smoothly as weight is transferred through the foot. To prevent numerical discontinuities (abrupt changes in force magnitude), the smoothstep windowing was applied as 4% of the stride time. This parameter caused a gradual increase and decrease in GRF during foot strike and toe-off. GRF only acted during the stance phase; during the swing phase, GRF was 0.

Once GRF was defined, it was combined with the limbs' instantaneous geometry—joint angles and segment positions—to calculate external knee moment at each timestep through the same procedure detailed in Section 2.1.3.

2.2.4 Output and Visualization

Producing visual and quantitative outputs allowed for an easier comparison of knee torque values. The Python libraries `numpy`, `matplotlib.pyplot`, and `matplotlib.gridspec` were utilized to create Figure 2.

2.3 Sensitivity Analysis — Evaluation of Parameter Influence on Model Robustness

Because *D. antirrhopus* is an extinct species, accurate and recorded measurements for key biomechanical inputs—like knee joint rest angle, passive elastic support (linear/cubic stiffness k_1 and k_3), *CoP* location, patellar tendon moment arm, and joint-angle keyframes—are scarce or nonexistent (Hutchinson, 2011). To ensure that results were not dependent on parameter assumptions, a sensitivity analysis was conducted. Inputs were systematically varied to quantify their influence on computed knee torque and quadriceps demand.

The parameters that were selected for perturbation affected moment arm geometry, and subsequently, the magnitude of the required F_{quad}. While there were other parameters that could have been tested, the following chosen had the most direct influence on quadriceps force.

1. Center of Mass (CoM_x)

   The range tested for the x-coordinate of the center of mass was $\pm$25% of the baseline horizontal position. Displacing the CoM_x altered the GRF's line of action relative to the knee joint, changing the external moment arm length in the torque equation. As the GRF force is relatively vertical, varying CoM_x resulted in a more significant sensitivity test than CoM_y —perpendicular variation to GRF affected its line of action to a greater extent. Testing CoM_x allowed for an examination of the effect of the anterior-posterior body mass distribution on F_{quad}. A forward-shifted (away from

the origin) CoM_x is expected to raise F_{quad} as ϕ (the GRF angle relative to the hip) increases, while a reverse shift (towards the origin, resulting in a more vertical stance) should decrease it.

2. Patellar Tendon Moment Arm (r_{pt})

   The range tested for the patellar tendon moment arm was $\pm$25% of the baseline r_{pt} for each respective species (0.0656 L_{femur} for *D. antirrhopus*; 0.09 L_{femur} for *S. camelus*). Testing the geometric sensitivity of the extensor mechanism allows more comparisons to be made on angular posture and energy-conservative positions. Because r_{pt} was a constant inversely related to F_{quad}, increasing it reduces quadriceps force and vice versa. r_{pt} was an essential parameter to test, as it not only acts as the mechanical lever arm, but also substantial data for the *D. antirrhopus* r_{pt} value is not present in existing literature (Hutchinson, 2005).

3. Knee Rest Angle (θ_0)

   For the knee rest angle, or the default angle of the knee joint, the range tested was $\pm$10º from baseline (55° for *D. antirrhopus*; 32° for *S. camelus*). Knee rest angle was perturbed to investigate how the neutral (solely ligament-supported) knee configuration influences passive torque contribution and equilibrium posture. The equation $M_{passive} = k_1(\theta_k - \theta_0) + k_3(\theta_k - \theta_0)^3$ was shifted, resulting in a change of the point where tendon support offsets gravitational and GRF moments. Altering θ_0 should shift the position of minimal muscle demand. The knee rest angle of both species is not a standardized value, so perturbation of this parameter was essential in a sensitivity test.

These parameters were respectively selected because of their effect on optimal torque positions and because their initialized values stemmed from relative assumptions off of scarce existing literature. Evaluating the robustness and biological realism of the created biomechanical model was essential to adding credibility to this study. Because extinct taxa lack complete experimental data, several anatomical and kinematic parameters must be estimated from comparative anatomy and indirect evidence. Small errors or discrepancies can propagate through the torque equation workflow. Sensitivity tests help to prove a minimal consequence of these effects.

Systematically varying the three chosen parameters within biologically plausible ranges, the sensitivity analysis quantified how much each variable influenced quadriceps demand. This demonstrated that comparative trends between *S. camelus* and *D. antirrhopus* remained stable under reasonable anatomical uncertainty and that conclusions on evolutionary mechanical optimization were not affected by single assumed values.

Results and Discussion:

3.1 Static Torque Optimization

Heatmaps of F_{quad} were generated for both *S. camelus* and *D. antirrhopus* models (Figure 1), and a comparison between the two revealed variations in muscle demand across different knee-ankle angle matrices. Figure 1 visualizes how much muscle force would be required to maintain different combinations of knee and ankle angles.

The *S. camelus* model exhibited a broader region of low muscle demand, centered on a semi-extended stance (knee 95°–110°, ankle 0°–40°), indicating an energy-efficient, semi-extended stance consistent with its real-world posture during standing and slow locomotion. The *D. antirrhopus* model, in comparison, exhibited a narrower and more flexed torque minimum (knee 115°–130°, ankle 0°–25°); this model produced higher average knee torques and F_{quad} values than the S. camelus model, reflecting greater muscular effort to maintain support.

These trends suggest that *S. camelus* maintains a higher efficiency across a wider variety of stance postures, where *D. antirrhopus* required more precise joint configurations to achieve a mechanical equilibrium. As the *D. antirrhopus* model required approximately 25–30% higher normalized F_{quad} at equivalent knee-ankle angle matrices, conclusions can be drawn to the fact that *D. antirrhopus* required a greater energy expenditure during stance.

The contrasting torque profiles indicate that limb posture/segment proportions strongly affect mechanical efficiency. The model cohesively demonstrates that evolutionary elongation of distal limb segments and anterior shifting of CoM reduced the mechanical cost of stance—a key adaptation in avian cursorial evolution.

Graph analysis demonstrates that ankle angle variation has a minimal effect on F_{quad} magnitude, especially in comparison to the knee angle. This aligns with expectations as the knee angle is closely correlated with motion; it also varies more during a single stride, further indicating it plays a more central role in determining F_{quad} than the ankle angle.

Code outputs for optimal knee and ankle angle are indicative of the positional stances of both *D. antirrhopus* and *S. camelus*. As a knee angle of 0° was initialized as a completely vertical posture, the greater angle magnitude of *D. antirrhopus* correlates with its more crouched posture, and the smaller angle magnitude of *S. camelus* correlates with its more vertical posture. These data points support the general finding that a more vertical positioning of joint angles minimizes F_{quad} and is more energy-efficient (Struzik et al., 2021).

Figure 1: Heatmaps showing normalized quadriceps force ($\frac{F_{quad}}{BW}$) across knee and ankle joint angles in *D. antirrhopus* (above) and *S. camelus* (below). Purple regions represent minimal torque zones, indicating an optimal mechanical efficiency. Optimal angles were computed via the Python models.

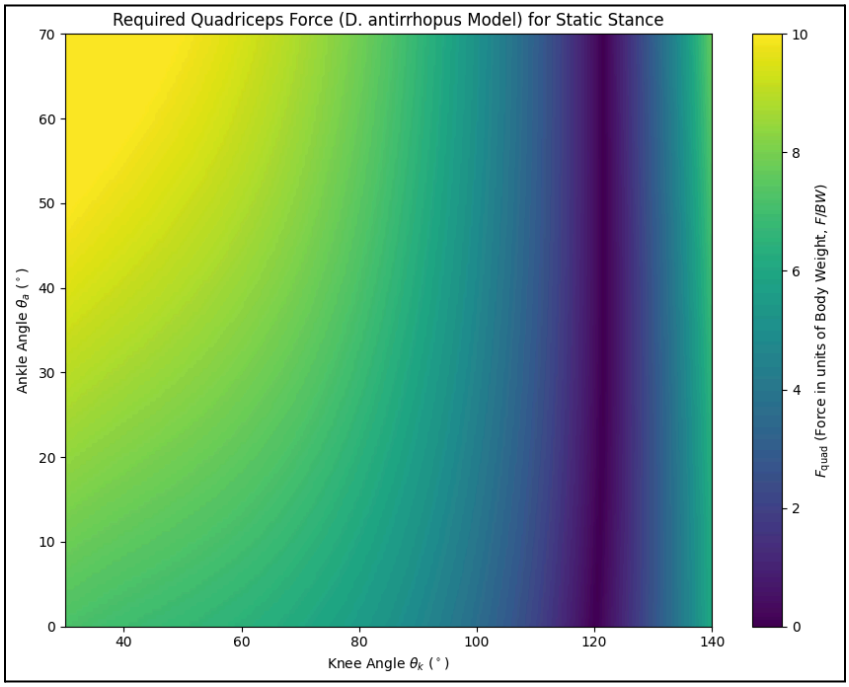

Optimal knee angle:
121.58371040723982°

Optimal ankle angle:
31.27659574468085°

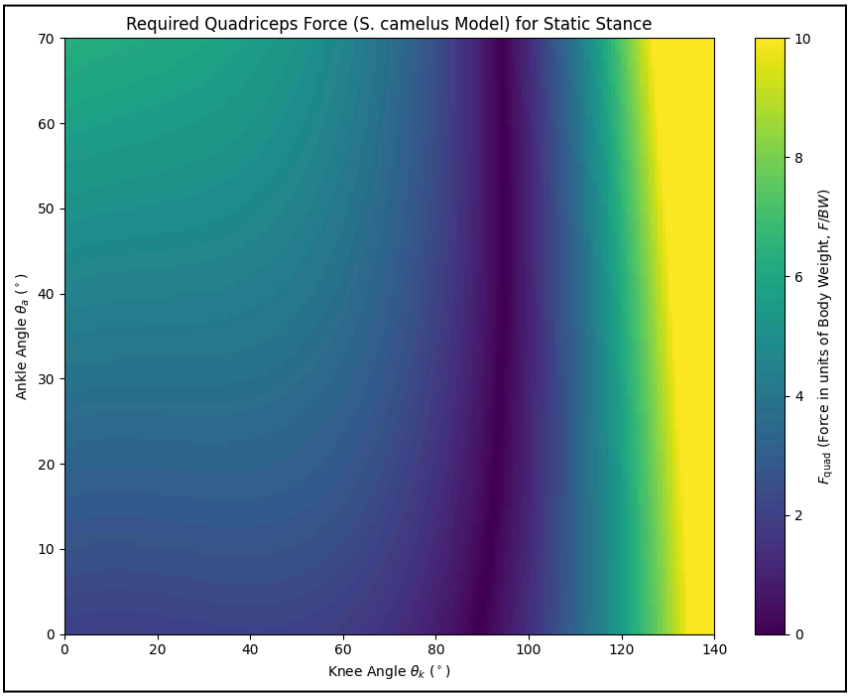

Optimal knee angle:
94.3646408839779°

Optimal ankle angle:
65.53191489361701°

3.2 Dynamic Stride Simulation

Results that were extrapolated from this section were joint angle profiles, knee moment trends, and quadriceps force.

Both *D. antirrhopus* and *S. camelus* exhibited fluctuations in joint angles over one stride. In the *S. camelus* model, these fluctuations were smoother; eased transitions between flexion and extension reflected a stable, more energy–efficient motion. In the *D. antirrhopus* model, greater angle amplitudes reflected significantly more variation, which is consistent with a more crouched, power-based gait.

Peak external knee moments occurred close to mid-stance for both species, aligning with a maximum GRF load and static torque minima. The combination of higher magnitude and sharper peaks for the *D. antirrhopus* model strongly supports a greater mechanical effort per stride, whereas the broader and lower-amplitude curves of the *S. camelus* model indicate a smoother load distribution and, consequently, a more efficient mechanical structure.

Force demand peaked near mid-stance for both species (~6 a.u (arbitrary units) for *D. antirrhopus*, and ~2 a.u for *S. camelus*), and declined towards toe-off, which was expected in accordance with when the GRF acts. *S. camelus* maintained a mean normalized F_{quad} value of 1.623 a.u.; *D. antirrhopus*, 2.732 a.u.. This 68.33% difference in mean F_{quad} values implies that *S. camelus* had a significantly higher dynamic leverage and efficiency than that of the *D. antirrhopus* model, whose higher peaks indicate a greater instability during load transfer.

Graphical analysis reveals the much greater angle and force fluctuations in the *D. antirrhopus* model, alongside a higher peak F_{quad} value. This rougher mechanical profile of *D. antirrhopus* suggests a morphology optimized for rapid force production rather than sustained efficiency. The contrasting S. camelus profile supports the hypothesis that evolution has directed towards optimizing *S. camelus* for continuous energy recovery and endurance.

Figure 2: Limb postures, joint angles, knee moments, and normalized quadriceps forces are shown across one stride (t = 0–1). Shaded areas denote the stance phase, or where the foot segment is in contact with the ground. *S. camelus* displays smoother, lower torque fluctuations, indicating higher dynamic efficiency, while *D. antirrhopus* shows sharper peaks, reflecting greater muscular demand.

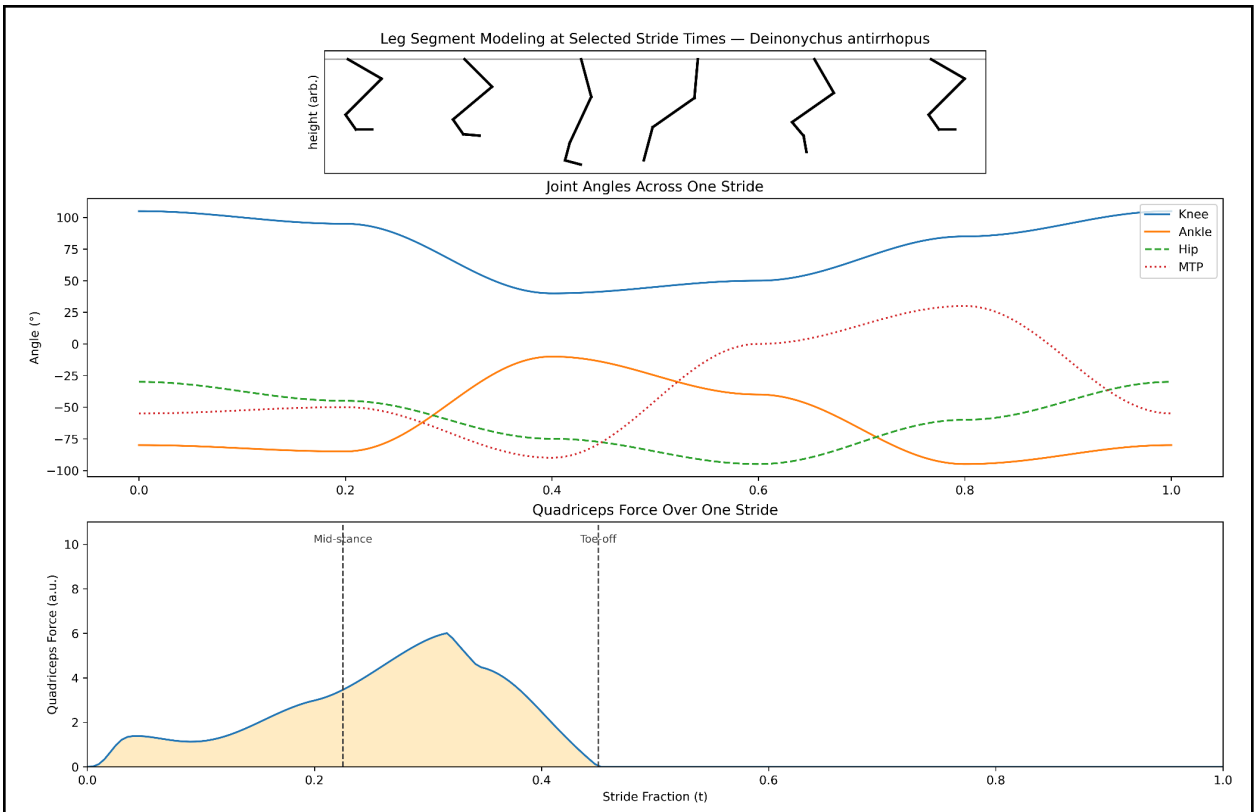
Leg Segment Modeling at Selected Stride Times — Deinonychus antirrhopus
height (arb.)
Joint Angles Across One Stride
Angle (°)
Knee
Ankle
Hip
MTP
Quadriceps Force Over One Stride
Quadriceps Force (a.u.)
Mid-stance
Toe-off
Stride Fraction (t)

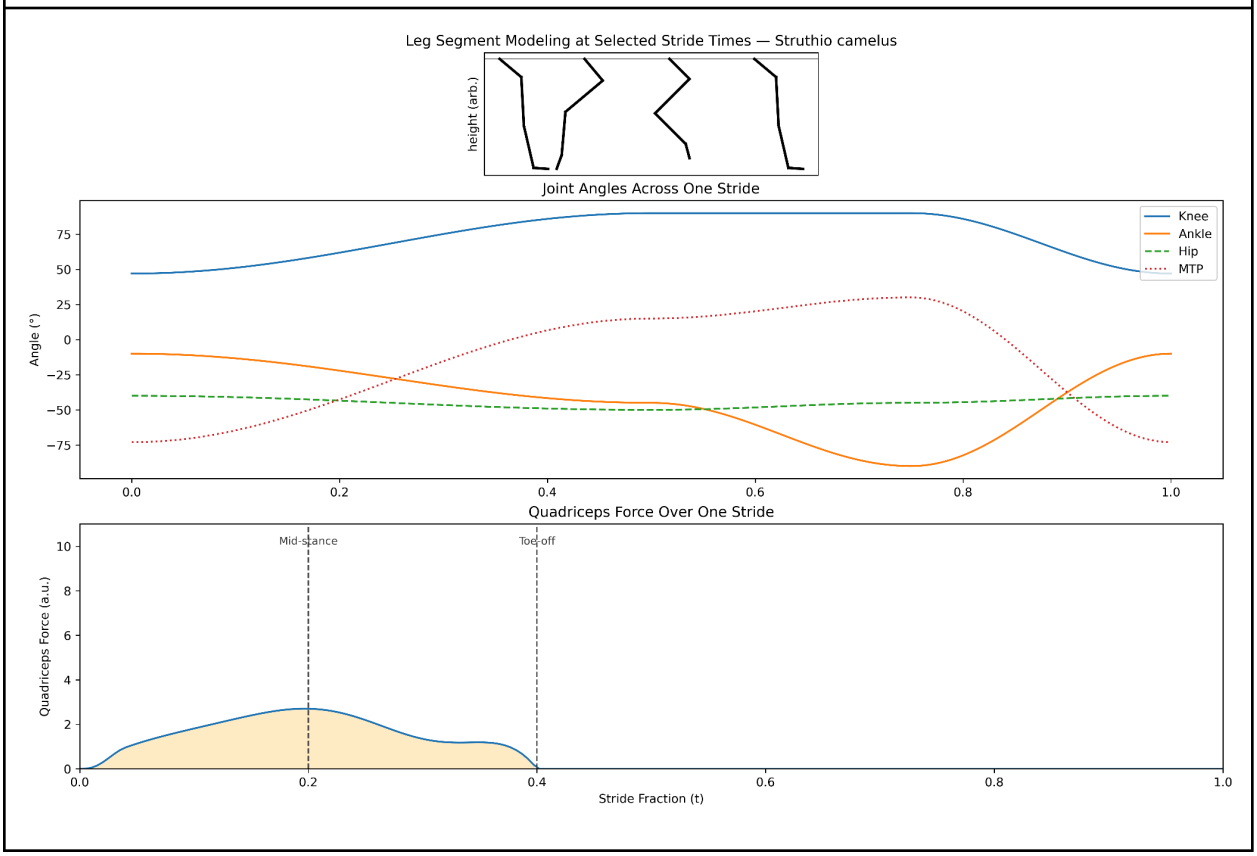
Leg Segment Modeling at Selected Stride Times — Struthio camelus
height (arb.)
Joint Angles Across One Stride
Angle (°)
Knee
Ankle
Hip
MTP
Quadriceps Force Over One Stride
Quadriceps Force (a.u.)
Mid-stance
Toe-off
Stride Fraction (t)

3.3 Sensitivity Analyses

Sensitivity tests quantified how changes in key biomechanical parameters—center of mass position (CoM_x), patellar tendon moment arm (r_{pt}), and knee rest angle (θ_0)—affected mean normalized F_{quad} values to ensure that model conclusions were not overly dependent on assumed anatomical inputs.

CoM_x Perturbation: Varying the horizontal position of the center of mass produced only minor fluctuations in F_{quad}, indicating that small anterior or posterior shifts have a minimal influence on knee demand. GRF line-of-action changes due to CoM_x offsets with this range do not strongly alter overall moment balance.

Patellar Tendon Moment Arm: Perturbing r_{pt} showed a near-symmetric response: decreasing the moment arm increased F_{quad} by a similar amount. This test reinforced the inverse relationship between tendon leverage and muscle force. Because the magnitude of this effect was relatively consistent across both species, the approximation of the moment arm value was validated.

Knee Rest Angle: Fluctuations in θ_0 exhibited the strongest influence on F_{quad}, with ~ 25% change in mean values. Increasing θ_0 raised F_{quad}, whereas decreasing θ_0 reduced muscular demand. The increase in F_{quad} values for the *D. antirrhopus* model when θ_0 was varied both positively and negatively signals that its crouched geometry makes it highly sensitive to joint-angle perturbations, while *S. camelus*—with a more erect and energy-optimized limb—exhibits greater mechanical stability.

Both taxa exhibited nearly identical directional trends, confirming model stability and a strong parameter approximation. As *S. camelus* displayed smoother response slopes, it can be inferred that it possessed more robust mechanics compared to the *D. antirrhopus* model, which relied more on a posture-dependent equilibrium.

Across the parameter perturbations, no reversal occurred, and trends stayed consistent. The dominance of θ_0 sensitivity emphasized its integral role in determining F_{quad} during stride movements. These results validate the two models' robustness: energy-efficiency trends between *D. antirrhopus* and *S. camelus* remain stable under plausible uncertainty.

Figure 3: Sensitivity plots showing percent change in mean normalized quadriceps force (ΔF_{quad}) relative to baseline for *D. antirrhopus* and *S. camelus*. Blue = CoM_x shift; Green = r_{pt} variation; Red = θ_0 perturbation.

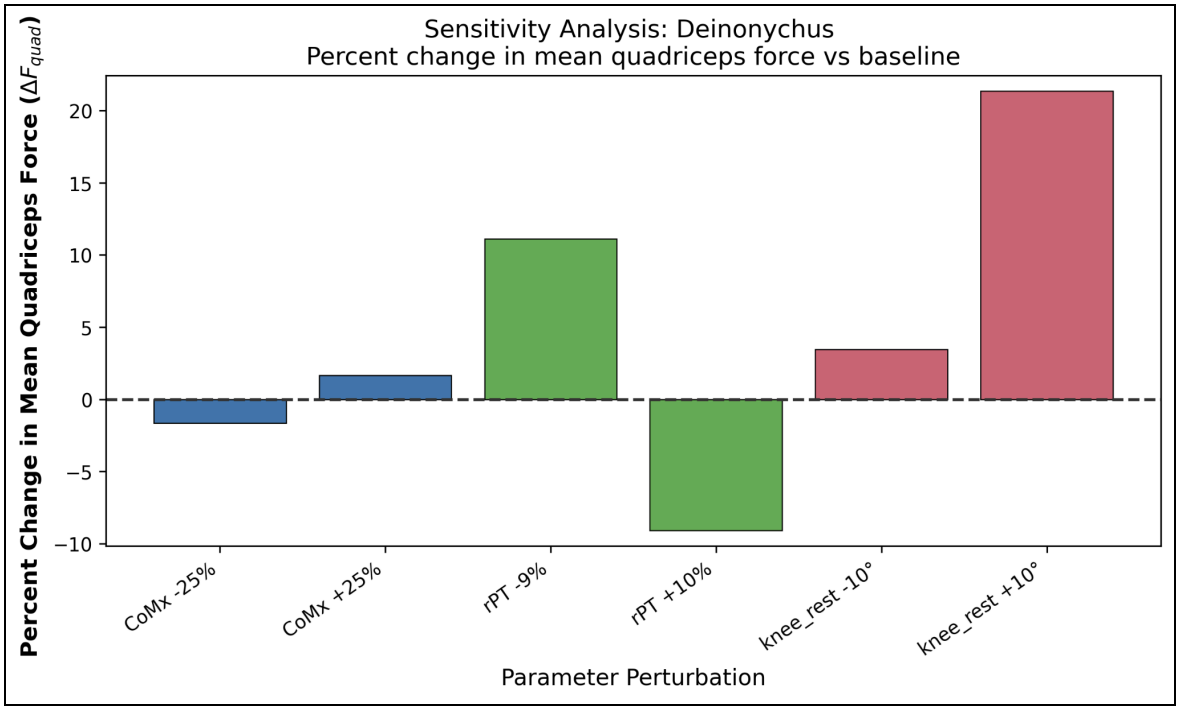

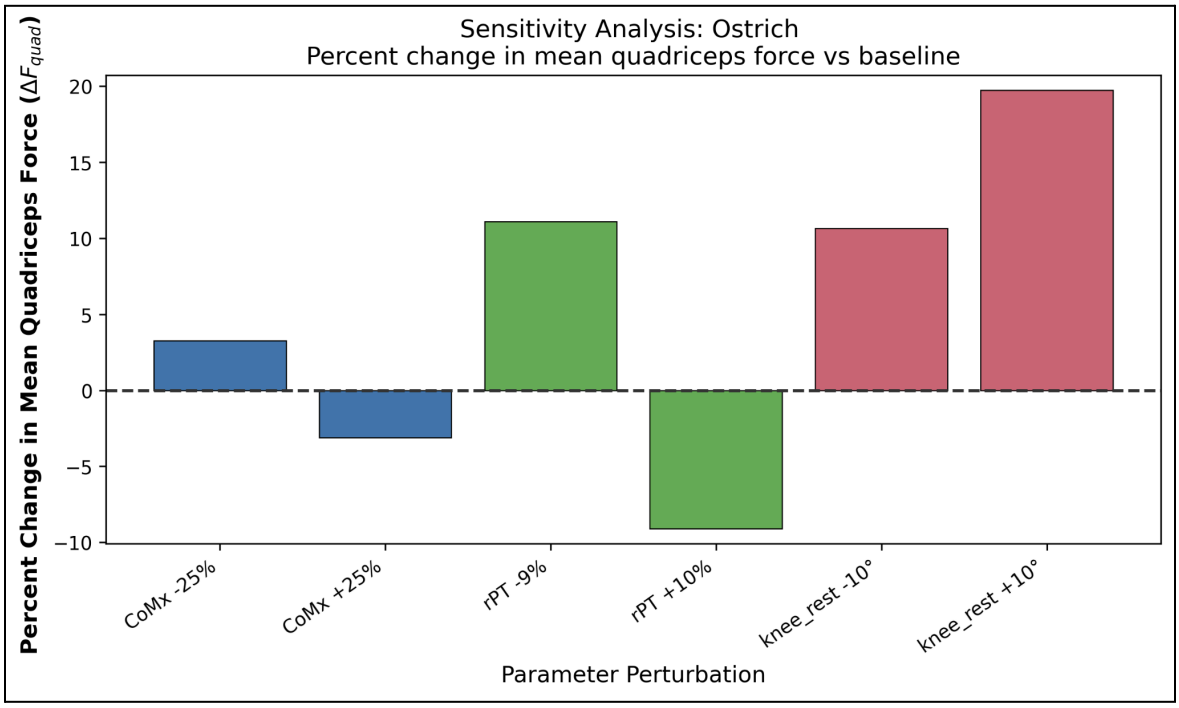

Overall Findings and Novelty:

Together, the combined results of this paper support the hypothesis that avian cursorial evolution has favored structural and positional modifications—especially elongated distal segments, a more vertical posture, and reduced flexion—that minimize energetic cost. Evolution does not work to "optimize" any organism; instead, "optimization" here is a general term for the processes of natural selection favoring energy efficiency over time. Thus, it can be reasoned that the clear evidence that *S. camelus* adapted for an environment where a more energy-efficient locomotive state makes biological sense; as the modern ostrich is a prey animal, traits that improved energy efficiency and endurance were selected for, optimizing *S. camelus* for its modern-day environment. In *D. antirrhopus*, a predator that lived in forested areas, selection favored locomotor traits for energetic bursts, as seen in modern-day predators (Fowler et al., 2011). In short, *S. camelus* represents an evolutionary continuation of locomotive changes that lead to greater stability and energy efficiency through cursorial optimization—for a modern niche (Rankin et al., 2016).

Limitations:

This study contains limitations due to the nature of comparative biomechanics with an extinct taxon. Firstly, because this study was conducted using simplified 2D static and dynamic models, results represent quantitative trends rather than precise biomechanical outputs. Similarly, because parameters were approximated, even with a sensitivity test, they do not reflect exact outputs. For *D. antirrhopus*, multiple constants—k_1, k_3, Θ_0, r_{pt}, and centers of mass and pressure—were estimated using extant taxa references and biologically logical assumptions derived from existing literature and known evolutionary trends.

Novelty:

The novelty of this originates from its interdisciplinary roots. Biological optimization processes (such as cursorial evolution) and their subsequent validations offer insights for bio-inspired robots and prosthetic designs, where identifying the locations of joint torque minima improves energy return. From an evolutionary biology standpoint, these findings add to the discussion of a biological economy–the trade-off between speed, stability, endurance, and power in cursorial evolution. By reinforcing that evolution can be modeled computationally, this study suggests evolution can be generally tracked and modeled as an optimization algorithm (though it is important to note that organisms do not evolve to become perfectly optimal). This study therefore combines paleontological reconstruction with computational biomechanics to test whether evolutionary elongation of distal segments—a key avian

cursorial adaptation—reduced mechanical cost during stance, providing quantitative support for the optimization-like processes of energy-efficient evolution in cursorial lineages.

Code Availability:

All Python code used for static torque analysis, dynamic stride simulation, and sensitivity testing is available through: https://doi.org/10.5281/zenodo.17685851

Data Availability:

All data used in this study can be regenerated from the accompanying Python code; example outputs are available in the linked repository.

Competing Interests:

The author declares no competing financial or non-financial interests.

Funding:

This research received no external funding and was conducted independently.

Author Contributions:

S.V. designed the study, developed the computational models, performed all analyses, and wrote the manuscript.

Acknowledgements:

The author thanks the online paleobiology and biomechanics community for publicly available datasets and skeletal reconstructions, namely Dr. Scott Hartman's Skeletal Drawings, that informed this computational work.

Appendix:

Table 1: All variable values were derived from existing literature. Segment lengths are expressed as dimensionless ratios relative to femur length. CoM coordinates are normalized to femur length, and defined as relative to the hip joint origin. Stiffness coefficients k_1 and k_3 follow nonlinear passive knee torque models from Regnault et al. (2017) and Hosseinzadeh et al. (2020), with logical approximates for the extinct taxa.

Variable	L_{femur} Femur Ratio	L_{tibia} Tibia Ratio	L_{met} Metatarsus Ratio	L_{pha} Phalanges Ratio	CoP Center of Pressure Fraction	CoM Center of Mass
D. antirrhopus	1.0	1.31242	0.46217	0.41785	0.6	(-0.05, 0.25)
S. camelus	1.0	1.71850	1.53003	0.51851	0.5	(0.08, 0.30)
Variable	θ_H Hip Angle	θ_{MTP} MTP Angle	r_{pt} Patellar Moment Arm	k_1	k_3	θ_0 Knee Rest Deg
D. antirrhopus	25°	-5°	0.0656	0.7	0.1	55°
S. camelus	35°	-10°	0.09	0.6	0.1	32°

Citations:

Allen, V. R., Bates, K. T., Li, Z., & Hutchinson, J. R. (2013). *Linking the evolution of body shape and locomotor biomechanics in bird-line archosaurs. Nature, 497*(7447), 104–107. https://doi.org/10.1038/nature12059

Allen, V. R., Hutchinson, J. R., Smith, N. C., & others. (2021). *The evolution of pelvic limb muscle moment arms in bird-line archosaurs. Proceedings of the Royal Society B.* https://pmc.ncbi.nlm.nih.gov/articles/PMC7978429/

Bishop, P. J., Cuff, A. R., & Hutchinson, J. R. (2021). *How to build a dinosaur: Musculoskeletal modeling and simulation of locomotor biomechanics in extinct animals. Paleobiology, 47*(1), 1–38. https://doi.org/10.1017/pab.2020.46

Castle, S. D., Stock, M., & Gorochowski, T. E. (2024). *Engineering is evolution: A perspective on design processes to engineer biology. Nature Communications, 15,* 3640.

Fowler, D. W., Freedman, E. A., Scannella, J. B., & Kambic, R. E. (2011). *The predatory ecology of Deinonychus and the origin of flapping in birds. PLoS ONE, 6*(12), e28964. https://doi.org/10.1371/journal.pone.0028964

Hartman, S. (n.d.). *Dr. Scott Hartman's Skeletal Drawing.com: The science and art of paleontology.* Retrieved October 4, 2025, from https://www.skeletaldrawing.com/

Hosseinzadeh, S., Barzegari, A., Taghipour, M., Mehr Aein, R., & Gholinia, H. (2020). *Changes of the patellar tendon moment arm length in different knee angles: A biomechanical in vivo study. Archives of Bone and Joint Surgery, 8*(5), 641–645. https://doi.org/10.22038/abjs.2020.42551.2158

Hutchinson, J. R. (2006). *The evolution of locomotion in archosaurs. Comptes Rendus Palevol, 5*(3–4), 519–530. https://doi.org/10.1016/j.crpv.2005.09.002

Hutchinson, J. R. (2012). *On the inference of function from structure using biomechanical modelling and simulation of extinct organisms. Biology Letters, 8*(1), 115–118. https://doi.org/10.1098/rsbl.2011.0399

Hutchinson, J. R., Anderson, F. C., Blemker, S. S., & Delp, S. L. (2005). *Analysis of hindlimb muscle moment arms in Tyrannosaurus rex using a three-dimensional musculoskeletal computer model: Implications for stance, gait, and speed. Paleobiology, 31*(4), 676–701. https://doi.org/10.1666/04044.1

Kassem, M. A. M., Tahon, R. R., Khalil, K. M., & colleagues. (2023). *Morphometric studies on the appendicular bony skeleton of the ostriches (Struthio camelus). BMC Veterinary Research, 19,* 109. https://doi.org/10.1186/s12917-023-03665-6

Kocher, C. D., & Dill, K. A. (2023). *Darwinian evolution as a dynamical principle. Proceedings of the National Academy of Sciences of the United States of America, 120*(11), e2218390120. https://doi.org/10.1073/pnas.2218390120

Kubo, T., & Kobayashi, Y. (2025). *Cursorial ecomorphology and temporal patterns in theropod dinosaur evolution during the mid-Cretaceous. Cretaceous Research, 161,* 105678. https://dinodata.de/bibliothek/pdf_c/2025/kubo-kobayashi-2025-cursorial-ecomorphology-and-temporal-patterns-in-theropod-dinosaur-evolution-during-the-mid.pdf

Rankin, J. W., Rubenson, J., & Hutchinson, J. R. (2016). *Inferring muscle functional roles of the ostrich pelvic limb during walking and running using computer optimization. Journal of the Royal Society Interface, 13*(118), 20160035. https://doi.org/10.1098/rsif.2016.0035

Regnault, S., Allen, V. R., Chadwick, K. P., & Hutchinson, J. R. (2017). *Analysis of the moment arms and kinematics of ostrich (Struthio camelus) double patellar sesamoids. Journal of Experimental Zoology Part A: Ecological and Integrative Physiology, 327*(4), 163–171. https://doi.org/10.1002/jez.2082

Rubenson, J., Lloyd, D. G., Besier, T. F., Heliams, D. B., & Fournier, P. A. (2007). *Running in ostriches (Struthio camelus): Three-dimensional joint axes alignment and joint kinematics. Journal of Experimental Biology, 210*(14), 2548–2562. https://doi.org/10.1242/jeb.004498

Seok, S., Wang, A., Chuah, M. Y., Hyun, D. J., Lee, J., Otten, D., Lang, J., & Kim, S. (2015). *Design principles for energy-efficient legged locomotion and implementation on the MIT Cheetah robot. IEEE/ASME Transactions on Mechatronics, 20*(3), 1117–1129. https://doi.org/10.1109/TMECH.2014.2339013

Smith, N. C., Payne, R. C., Jespers, K. J., & Wilson, A. M. (2007). *Muscle moment arms of pelvic limb muscles of the ostrich (Struthio camelus). Journal of Anatomy, 211*(3), 313–324. https://doi.org/10.1111/j.1469-7580.2007.00762.x

Struzik, A., Karamanidis, K., Lorimer, A., Keogh, J. W. L., & Gajewski, J. (2021). *Application of leg, vertical, and joint stiffness in running performance: A literature overview. Applied Bionics and Biomechanics, 2021,* 9914278. https://doi.org/10.1155/2021/9914278

Taylor, P. D. (1990). *Optimality theory in evolutionary biology. Nature, 348*(6298), 27–33. https://doi.org/10.1038/348027a0

Zhang, R., Ji, Q., Luo, G., Xue, S., Ma, S., Li, J., & Ren, L. (2017). *Phalangeal joints kinematics during ostrich (Struthio camelus) locomotion. PeerJ, 5,* e2857. https://doi.org/10.7717/peerj.2857